WARSAW UNIVERSITY OF TECHNOLOGY Index 351733
FACULTY OF CIVIL ENGINEERING
COMMITTEE FOR CIVIL AND WATER ENGINEERING
POLISH ACADEMY OF SCIENCES ISSN 1230-2945

DOI: 10.24425/ace.2022.143055

ARCHIVES OF CIVIL ENGINEERING

Vol. LXVIII ISSUE 4 2022

pp. 571 –590

Research paper

Damage mechanism of conventional joints and proposal of a novel joint for hollow-core slab bridges

Yujun Cui[1], Xingwei Xue[2], Hao Yao[3], Xudong Hua[4], Yuanming Huang[5]

Abstract: The prefabricated hollow-core slab bridge is a common bridge. In prefabricated hollow-core slab bridges, joints play an important role in connecting prefabricated slabs and ensuring the integrity of the bridge. However, as the service time of the bridge increases, conventional joints have a large number of typical diseases that affect the safety and durability of bridges. In this study, a three-dimensional finite element model of the entire construction phase is established to investigate the development difference of shrinkage and creep between joints and hollow-core slabs. The effects of vehicle load and temperature gradient on joints were analysed, the failure mechanism of joints was explored, and a novel joint was proposed. The results of a nonlinear analysis showed that the novel joint can effectively improve the mechanical performance of joints and cracks can be effectively controlled. Moreover, the novel joint solves the problem in that the conventional novel joint cannot be vibrated effectively.

Keywords: a novel joint, failure mechanism, joint, prefabricated hollow-core slab, shrinkage and creep, vehicle load and temperature gradient

[1]M.Sc., Eng., School of Transportation and Surveying Engineering, Shenyang Jianzhu University, Shenyang, Liaoning, China, e-mail: 1789729061@qq.com, ORCID: 0000-0001-6494-5335
[2]Prof., PhD., School of Transportation and Surveying Engineering, Shenyang Jianzhu University, Shenyang, Liaoning, China, e-mail: gdansys@163.com, ORCID: 0000-0002-8605-1196
[3]M.Sc., Eng., Guangzhou Communications Investment Group Co., Ltd., Guangzhou, Guangdong, China, e-mail: yyaohao@foxmail.com, ORCID: 0000-0003-3659-9193
[4]M.Sc., Eng., School of Transportation and Surveying Engineering, Shenyang Jianzhu University, Shenyang, Liaoning, China, e-mail: 15998232953@163.com, ORCID: 0000-0002-9923-2498
[5]M.Sc., Eng., School of Transportation and Surveying Engineering, Shenyang Jianzhu University, Shenyang, Liaoning, China, e-mail: 1397796361@qq.com, ORCID: 0000-0002-6040-1725

1. Introduction

Prefabricated hollow-core slabs have many advantages, such as low weight, low cost, convenient construction, and prefabrication favourability [1–5]. Therefore, they are widely used in bridge engineering, especially in bridges with spans of 10–20 m.

Cast-in-situ joints are placed between the prefabricated hollow-core slabs, and the cast-in-situ bridge deck is placed above the hollow-core slabs and joints. The prefabricated hollow-core slabs, joints, and bridge decks together form an overall structure to bear loads. Therefore, joints play an important role in the load transfer of the transverse bridge and overall stiffness of the bridge structure [6–10]. Figure 1 shows the structure of common joints, which are categorized into three types according to their depth: shallow, medium, and deep joints.

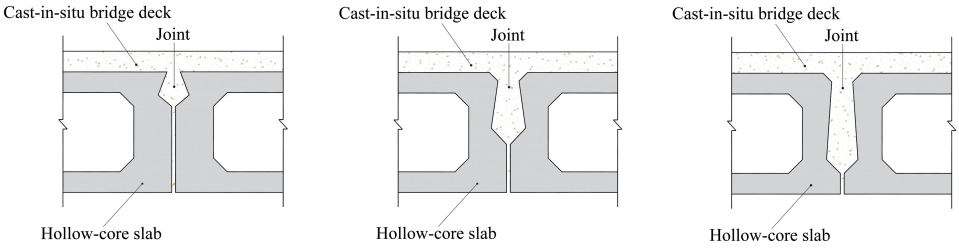

(a) Shallow joints (b) Medium joints (c) Deep joints

Fig. 1. Common forms of joints

The design of these joints has the following drawbacks. As these joints are small in size, their effective vibration is difficult. Furthermore, these joints are generally only equipped with hinged reinforcement, which cannot resist the transverse and longitudinal stress generated by loads, such as vehicles, leading to the formation of cracks. During service periods, various degrees of defects were observed, the most common being cracking and concrete shedding of joints (Figure 2a, 2b) [11–15]. When the joints are damaged, the transverse connection is weakened. This increases the loads on the hollow-core slabs, and consequently results in the formation of transverse cracks in the slabs (Figure 2c) and longitudinal cracks in the bridge deck (Figure 2d). These defects greatly reduce the durability and safety of the bridge [16, 17].

Some scholars have proposed improvements in the mechanical properties of joints to improve their working performance. Ultra-high performance concrete (UHPC) has excellent mechanical properties such as compression, tension, and toughness [18–20]. Jiang et al. [21] used UHPC as a joint material to enhance the shear strength. Yuan et al. [22] used UHPC as a joint grout material, and discussed and compared the mechanical properties of joints with different connection details. Semendary et al. [23] studied the early-age behaviour of a bridge containing partial-depth joints grouted with UHPC and equally spaced dowel bars. Hussein et al. [24] conducted direct shear, direct tension, and flexural tests on joints that used UHPC as the grout material. Issa et al. [25] carried out tests using solidification grouting, normal temperature solidification grouting, high-temperature solidification

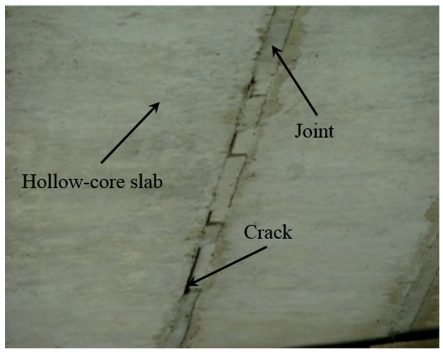

(a) Cracks of joints [15]

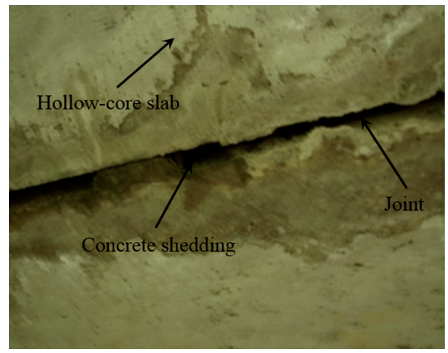

(b) Concrete shedding of joints [15]

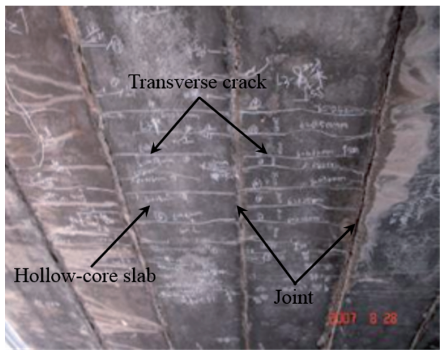

(c) Transverse cracks of hollow-ore slabs

(d) Longitudinal cracks of bridge deck

Fig. 2. Typical disease of joints and hollow-core slabs

grouting, and polymer concrete as joint grout materials. Direct shear, direct tension, and flexural tests were performed, and polymer concrete was recommended as the material for grouting joints.

Moreover, the age difference in shrinkage and creep development between prefabricated hollow-core slabs and post-cast joints may cause cracks. Shi et al. [26] used shrinkage-compensating cement as a joint grout material and performed experimental and numerical analyses. The results of both analyses showed that the stresses in the joint made with shrinkage-compensating cement concrete remained below the cracking threshold under temperature and shrinkage effects.

At the same time, structural optimisation of joints has also been studied considerably. Liu and Yang [27] and Wang [28] proposed increasing the thickness of the cast-in-situ bridge deck and adopted a joint bolt pin to transmit the transverse tensile stress. Annamalai et al. [29] applied transverse prestressed steel strands to prefabricated hollow-core slabs to improve the shear resistance of joints and enhance the integrity of the bridge. Yamane et al. [30] set the transverse diaphragm in a hollow-core slab bridge to allow the transverse prestressed steel strands to pass through the transverse diaphragm. This can enhance the

transverse force performance of the bridge and reduce the construction difficulty of applying transverse prestressed steel strands. The Turner-Fairbank Highway Research Center [21] designed a diamond-shaped joint, which uses UHPC as the grout material and is equipped with transverse reinforcement to overcome the disadvantages of longitudinal cracks, as shown in Figure 3.

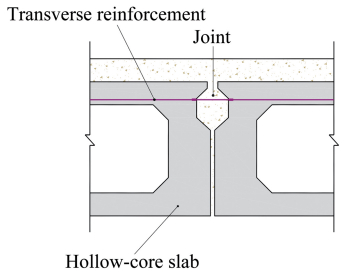

Fig. 3. Diamond-shaped joint

Zhong [15] conducted a numerical analysis to study the mechanical properties of joints. The research results showed that hinged and top-connecting reinforcements in joints can enhance the transverse connection performance of hollow-core slabs; this helps prevent cracking and improve the durability of the joints, as shown in Figure 4.

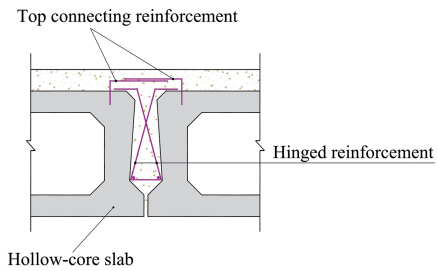

Fig. 4. Reinforced deep joint [14]

Joints play an important role in bridge structures. First, we explored the failure mechanism of the existing joints, considering the effects of concrete shrinkage and creep, vehicle loads and temperature loads on the mechanical properties of the joints, and then proposed a new type of joint against the typical diseases described earlier, which is equipped with steel reinforcement and increased size.

2. Model

2.1. Overview and linear model of bridge

A simply supported prestressed hollow-core-slab bridge has a span of 13 m and width of 8.5 m. Its vehicle load grade is highway-I. The superstructure is composed of six

prefabricated hollow-core slabs. The length, width, and height of a single hollow-core slab is 1296, 124, and 70 cm, respectively, and the thickness of the cast-in-situ bridge deck is 10 cm. Four supports are arranged at the bottom of the single hollow-core slab.

The bottom of the joint between the hollow-core slabs is 1-cm wide. The cross section of the hollow-core-slab bridge is shown in Figure 5, with joints labeled J1–J5 from left to right.

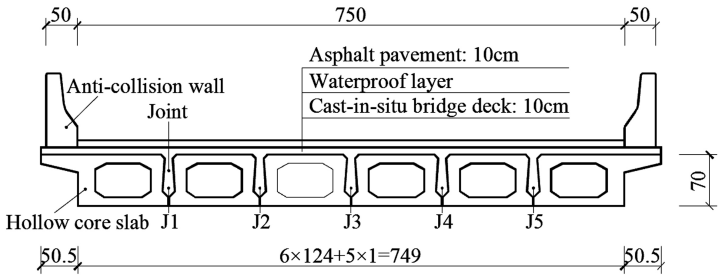

Fig. 5. Cross section of hollow-core slab bridge (Unit: cm)

The hollow-core slab, joints, and cast-in-situ layer of the bridge deck are all made of concrete with a strength grade of 50 MPa. Each prefabricated hollow-core slab was configured with 12 prestressed steel strands, and possesses a diameter of 15.2 mm and elastic modulus of $E_p = 1.95 \times 10^5$ MPa.

The loads considered in the mechanical analysis of the hollow-core slab included the following: (1) self-weight of the hollow-core slabs (SF1), self-weight of the cast-in-situ bridge deck and joint (SF2), and self-weight of the asphalt layer and anti-collision wall (SF3); (2) prestress of hollow core slabs (PS); (3) shrinkage and creep (CS); (4) temperature gradient (TG); and (5) vehicle load (VL).

Among them, loads (1)–(3) were applied during construction, and loads (4) and (5) were applied after the bridge was built. Loads (1) and (2) were applied according to the corresponding weight, and the introduction of loads (3)–(5) is detailed in Section 2.2.

A three-dimensional finite element model of a hollow-core-slab bridge was established with eight-node solid elements. The model comprises a total of 299,946 nodes and 278,176 elements.

Four stages were adopted to analyse the mechanical behaviour of joints, and the construction period from *stage i* to *stage iii* is assumed to take 120 days:

Stage i: Activate the hollow-core-slab structure. Apply loads SF1 and PS. The bulk density of the prefabricated hollow-core slab is 26 kN/m^3, and the prestressed tensile stress of the steel strand is 1395 MPa. Note that the hollow-core slabs at this stage have a certain age, such as 15 or 30 days.

Stage ii: Apply the self-weight of the cast-in-situ bridge deck and joints SF2 (4.35 kN/m^2) on the prefabricated hollow-core slabs. Because the concrete of the joints and cast-in-situ bridge deck has no strength when just poured and cannot bear the load, its self-weight is applied to the prefabricated hollow-core slabs in the form of wet weight.

Stage iii: Activate the structure of the joints and cast-in-situ bridge deck, and then apply load SF3 and CS. SF3 includes an anticollision wall (16 kN/m^2) and asphalt layer (2.4 kN/m^2), as shown in Figure 6a.

Stage iv: Apply VL and TG, as shown in Figure 6b.

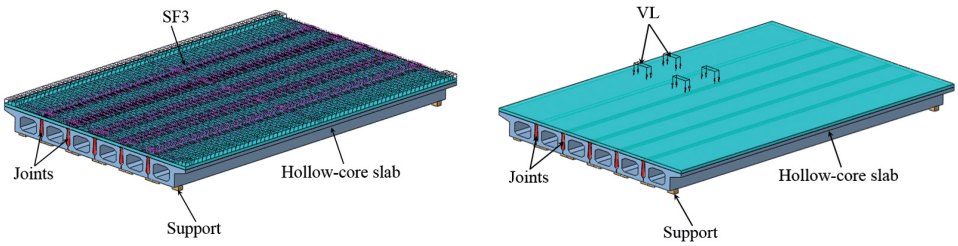

(a) *Stage iii* (b) *Stage iv*

Fig. 6. Model of hollow-core slab bridge

2.2. Load

2.2.1. Shrinkage and creep (CS)

In practice, after the hollow-core slab is prefabricated, the hoisting process could begin after dozens or even hundreds of days. During this period, the CS of the prefabricated hollow-core slabs could develop. Therefore, the difference in the development of CS occurs between the concrete of the prefabricated hollow-core slabs and the joints and bridge deck, the concrete of which is cast in place after the prefabricated hollow-core slabs are hoisted [31–35]. The difference in CS development between the different structures is an important reason for joint failure.

Shrink. When concrete hardens in air, its volume decreases. This phenomenon is called concrete shrinkage, and is is generally considered to be due to shrinkage of gel and water loss. The final shrinkage strain of ordinary concrete is approximately $(1-5)\times 10^{-4}$, which is three to five times the peak strain of its axial tension. Shrinkage is the main reason for the development of internal micro-cracks and external macro-cracks. The shrinkage strain, ε_{cs}, of concrete can be calculated according to Equation (2.1) [36]:

$$\varepsilon_{cs}(t,t_s) = \varepsilon_{cso}\beta_s(t-t_s) \tag{2.1}$$

where: t – shrinkage development time, t_s – age of concrete at the beginning of shrinkage, ε_{cso} – nominal shrinkage coefficient, β_s – development coefficient of shrinkage related to time.

Creep. Under long-term continuous stress, the phenomenon in which the deformation of concrete increases with time is called creep. This phenomenon could occur because of two reasons. On the one hand, the cement gel in the concrete generates viscous flow under the load and gradually transfers its pressure to the aggregate particles. This causes an increase in the compressive stress of the aggregate, which in turn causes an increase in the

deformation of the concrete specimen. On the other hand, the microcracks in the concrete continue to develop and increase under long-term loads. Creep is an important deformation performance of concrete under long-term loads. Creep causes stress redistribution between structures, increases the deformation of the compression zone of the flexural member, and increases the deflection of the flexural member. Creep coefficient of concrete can be calculated according to Equation (2.2) [36]:

$$\varphi(t, t_0) = \varphi_0 \cdot \beta_c(t - t_0) \tag{2.2}$$

where: t_0 – loading age of concrete, t – age of the concrete, $\varphi(t, t_0)$ – creep coefficient when the loading age is t_0 and the concrete age is t, φ_0 – nominal creep coefficient, β_c – coefficient of creep development with time after loading.

Figure 7 shows the longitudinal normal stress of joint J1 at the midspan section in *stage iii* when the ages of prefabricated hollow-core slabs are 15 days, 30 days, 90 days, 120 days, 1 year, and 2 years.

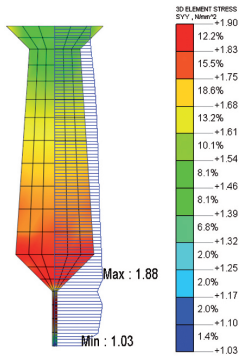

(a) Age of 15 days

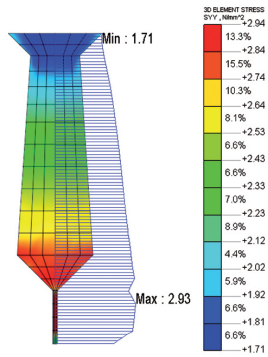

(b) Age of 30 days

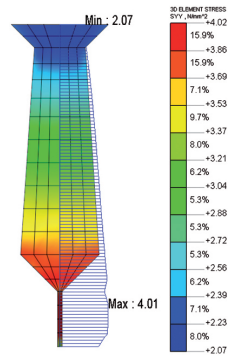

(c) Age of 60 days

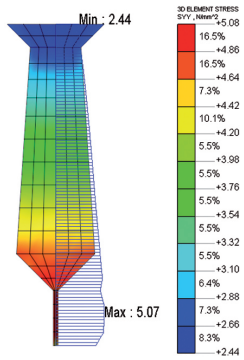

(d) Age of 120 days

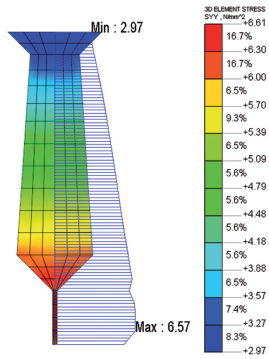

(e) Age of 1 year

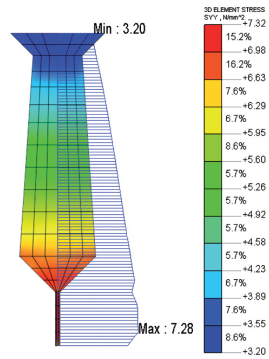

(f) Age of 2 years

Fig. 7. Longitudinal normal stress of J1 at mid-span section (unit: MPa)

As shown in Figure 7, after *stage iii*, entire sections of the joints of the prefabricated hollow-core slabs of different ages are under tensile stress. The tensile stress of joints is relatively high, and it tends to increase with age. Therefore, the bottom of the joints will inevitably crack after *stage iii*.

Figure 8 shows an elevated view of the longitudinal normal stress of joint J1 at 120 days. The joints at J1 and other positions show the same tendency; except for the supporting position, the distribution law and numerical value of the joints along the longitudinal bridge are consistent with the midspan section shown.

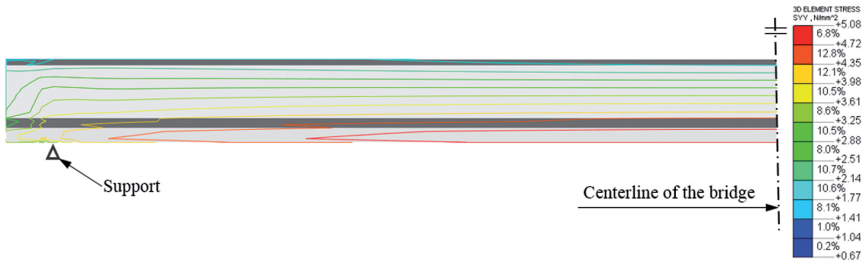

Fig. 8. Semi-elevation view of longitudinal normal stress of J1 (unit: MPa)

2.2.2. Temperature gradient (TG)

The temperature gradient causes longitudinal and transverse tension of the joint; this is an important reason for the cracking of the joint.

Under the action of a positive temperature gradient, apart from the compressive stress on the bottom of the joints, the joint mainly undergoes tensile stress. The compressive stress of the positive temperature gradient at the bottom of the joints can play a certain role in restraining the development of cracks, but its effect is not significant. The tensile stress in the middle part, after being combined with other loads, can play an important role in the propagation of cracks from the bottom to the top. If a negative temperature gradient is applied, the stress distribution is opposite to the positive temperature gradient, and the stress value is approximately −0.5 times the stress value of the positive temperature gradient. In comparison, a positive temperature gradient is more unfavourable for the failure of the joint.

In the analysis, the temperature gradient was taken from 0–100 mm as 14–5.5°C and 100–400 mm as 5.5–0°C [36]. Under the action of the temperature gradient, the stress distribution of each joint is consistent, and the stress of the joint remains unchanged along the longitudinal direction of the bridge. The longitudinal normal stress of the J1 midspan section under the action of the temperature gradient is shown in Figure 9.

As shown in Figure 9, under the effect of the temperature gradient, the mid-span section of J1 mainly undergoes tensile stress, and the maximum tensile stress is 1.11 MPa. Compressive stress is observed at the bottom of J1, with the maximum value of −0.74 MPa.

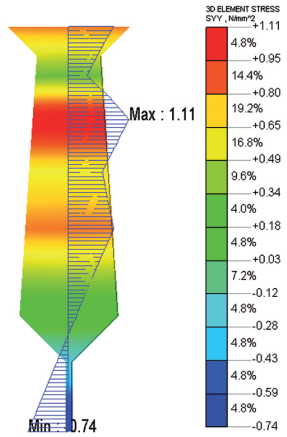

Fig. 9. Longitudinal normal stress of J1 at mid-span section under temperature load (unit: MPa)

2.2.3. Vehicle load (VL)

The VL can cause a relatively large longitudinal normal stress on the joint. The VL was selected according to a given specification with the weight of 55 t. It consists of a set of front axles and two sets of rear axles. A single rear axle wheel is 70 kN, and the width of the wheel landing is 60×20 cm. Therefore, the uniform load of a single wheel is $q = 584$ kN/m^2 [36].

The layout of the vehicle that moves J1 into the most unfavourable mechanical state occurs when the VL is applied symmetrically to the bridge span through the double rear axle. The arrangement that causes the VL to produce the greatest tensile stress in the joint occurs when the two rear axles are arranged symmetrically in the middle of the bridge span and are against the anticollision wall. The VL produced the greatest tensile stress in the joint, as shown in Figure 2b. Under the effect of the VL, the value of the longitudinal normal stress J1 is the largest. Figure 10 shows the longitudinal normal stress of the midspan section of J1. As shown in Figure 10, the longitudinal normal stress in J1 is a compressive stress above the neutral axis and a large tensile stress below the neutral axis.

The VL and temperature gradient are both the bridge loads in the service phase. We combine them to facilitate viewing of the effect of service phase loads. The load combination result of the longitudinal normal stress of J1 at the midspan section is shown in Figure 11.

The comparison of Figures 11 and 7 showed that after completion of bridge construction (*stage iii*), the joint is already in a very unfavourable mechanical state, and the maximum tensile stress caused by CS is 1.88–7.28 MPa. The maximum normal stress of the load combination of the VL and TG at J1 is 1.15 MPa. Therefore, the tensile stress in the joint is mainly caused by the difference in CS, followed by the VL and TG.

Regarding conventional joints, whether in *stage iii* or *stage iv*, the tensile stress in these joints exceeds the maximum allowable tensile stress of the concrete. Therefore, nonlinear analysis of the structure is required.

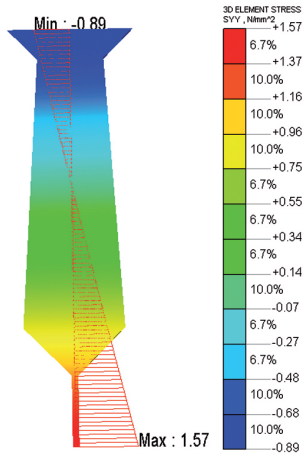

Fig. 10. Longitudinal normal stress of J1 at mid-span section under vehicle load (unit: MPa)

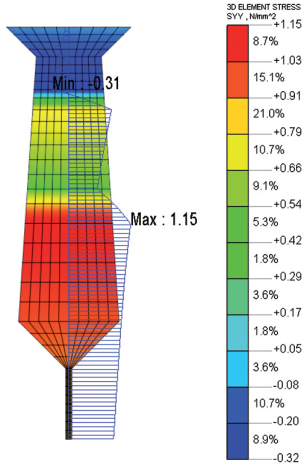

Fig. 11. Longitudinal normal stress of J1 at mid-span section under vehicle load and temperature load (unit: MPa)

3. Mechanism of joint failure

Owing to the effect of prestress, hollow-core slabs can maintain elasticity during service. However, the joint is very likely to crack owing to the load, shrinkage, creep, and temperature. Therefore, the joint must consider the nonlinearity of the concrete materials. This section discusses the mechanism of joint failure under various working conditions.

3.1. Constitutive relationship

(1) Concrete

In this study, a rotating crack model of the total strain crack model was used to simulate concrete, the advantages of which are as follows. (1) The crack distribution is convenient to show, and the crack unit does not separate at the crack position. (2) The crack direction changes with the direction of the main strain; only the normal stress is generated on the crack surface, and the calculation process is simpler.

The nonlinear properties of concrete under compression were assigned to the developed finite element models by defining the stress-strain relation developed using the parabolic hardening softening model [37–39], which depends on three parameters: concrete compressive strength f_c, concrete fracture energy G_c, and concrete characteristic element length h_c, as shown in Figure 12. The concrete compressive strength, f_c, concrete characteristic element length h_c, and elasticity modulus of concrete E_c can be obtained through experimental tests.

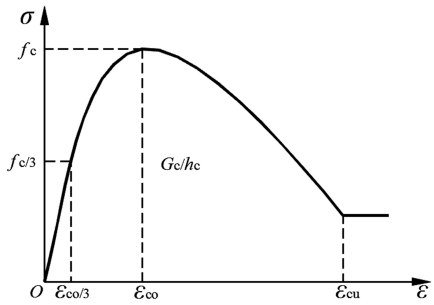

Fig. 12. Compression constitutive relations of parabolic model

G_c can be calculated according to Equation (3.1):

$$G_c = G_{co}\left(\frac{f_c}{f_{cmo}}\right)^{0.7} \tag{3.1}$$

where f_{cmo} is the benchmark average compressive strength, and its value is 10 N/mm^2. G_{co} is related to the maximum aggregate size, and the corresponding relationships are listed in Table 1.

Table 1. Relationship between G_{co} and maximum aggregate size

D_{max} (mm)	G_{co} (J/m^2)
8	23
16	30
32	58

The peak compressive strain, ε_{co}, corresponding to the concrete compressive strength, f_c, and the ultimate compression strain at the softening stage are expressed as Equation (3.2) and Equation (3.3).

$$\varepsilon_{co} = \frac{4}{3}\frac{f_c}{E_c} \tag{3.2}$$

$$\varepsilon_{cu} = \varepsilon_{co} - \frac{3}{2}\frac{G_c}{h_c f_c} \tag{3.3}$$

Tensile models of concrete in total strain crack models, such as constant, elastic, brittleness, linear, exponential, Hordijk, and multi-linear models, are provided in Midas/FEA. This study used a brittleness model [37–39], which considers the concrete tensile strength as the stress end point. When the concrete tensile stress value exceeds the tensile strength value, it does not increase, and the concrete resistance stress value tends to zero, as shown in Figure 13.

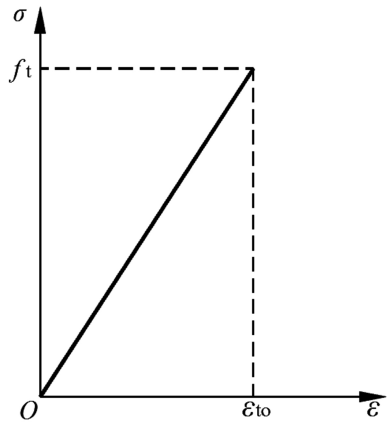

Fig. 13. Tension constitutive relationship of brittleness model

The constitutive model of the brittleness model includes two main parameters: the tensile strength value, f_t, and peak tensile strain, ε_{to}. Tensile strength f_t is obtained by testing or reference specifications, and extreme strain ε_{to} can be obtained according to Equation (3.4).

$$\varepsilon_{to} = 65 \times f_t^{0.54} \times 10^{-6} \tag{3.4}$$

(2) Steel bar

In this study, the reinforcement was modelled using embedded rebar elements that added the stiffness of the reinforcement to the parent elements. The basic properties of steel bars include information on the position, shape, and physical properties, without degrees of freedom. There was no slip between the rebar and parent elements, and the strain of the rebar elements was calculated according to the displacement of the parent elements.

The Von Mises model was adopted in the constitutive structure of steel bars and is provides good response to the mechanical properties of metal materials. The Von Mises model in Midas/FEA must define the hardening curve of the yield stress of the material. Generally, the hardening function is defined according to the material stress–strain curve given by the specification, and an ideal elastoplastic model is adopted. The ideal elastic-plastic model of the steel bar adopts the tri-polyline model, which can accurately simulate the stress-strain relationship of the steel bar that will undergo stress strengthening immediately after yielding [40]. In Figure 14, f_y is the yield strength of the steel bar, f_{st} is the ultimate strength of the steel bar, ε_y is the yield strain of the steel bar, ε_{uy} is the starting strain of the steel bar hardening, and ε_u is the peak strain of the steel bar.

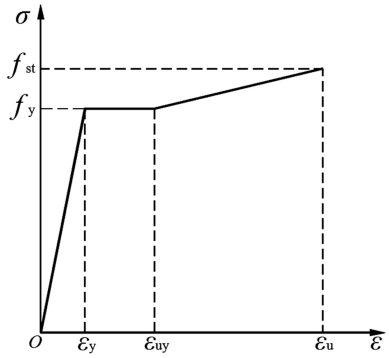

Fig. 14. Ideal elastic-plastic model of steel bar

3.2. Analysis of joint failure mechanism

The analysis in *Part 2* was a linear analysis, and shrinkage and creep could be considered. In the Midas/FEA program, material nonlinearity cannot be used simultaneously with CS, but it can be used with temperature.

To simulate the cracking of concrete, this study considers the CS development difference between prefabricated hollow-core slabs and joints by means of joint and bridge deck cooling. The principle of the difference in CS development between joint and bridge deck cooling is as follows. The difference in CS development between prefabricated hollow-core slabs and joints causes the joints to be tensile. This is consistent with the effect that the joint and bridge deck are constrained by prefabricated hollow-core slabs and then cooled. Through a large number of calculations, the effect of the joint cooling to 9.8°C is the same as the 120-day difference in CS between prefabricated hollow-core slabs and joints. Therefore, the effect of CS is replaced by the joints and bridge deck cooling at 9.8°C.

The effects of shrinkage and creep were replaced by cooling, and the material nonlinearity of concrete and steel was considered. The following section focuses on the analysis of crack development in J1. There is little difference between the development of cracks in *stages iii* and *iv*; therefore, only the joint cracks of *stage iv* are shown in Figure 15.

(a) Semi-elevation view of cracks

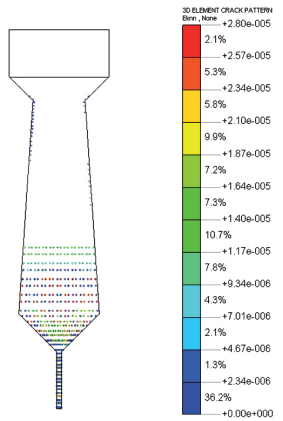

(b) Cracks at the mid-span cross section

Fig. 15. Crack distribution of J1 in *stage iv*

VLs and TGs are applied after the bridge construction is completed in *stage iv*. As shown in Figure 15a, the cracks are distributed in the middle and bottom parts of the entire joint, and the cracks in the middle and lower parts of the joint have penetrated (Figure 15b). In addition, the upper part of the joint comprised cracks, which are located at the junction of the joint and hollow-core slab. This shows that the cracks exhibited an upward trend. If the vehicle is overloaded or the CS development difference is more than 120 days, the cracks may develop upwards to the bridge deck, which will cause water seepage in the joints and longitudinal cracks in the bridge deck. This significantly weakens the overall stiffness of the bridge.

4. Novel joint and its mechanical characteristics

4.1. Structure of novel joints

Owing to their small size, conventional joints not only cause difficulty in concrete vibration but also cannot embed steel bars to resist the load. Under the effects of self-weight, shrinkage, creep, temperature, and vehicles, cracking of conventional joints becomes in-

evitable. Therefore, it is necessary to propose a new type of joint. A structural diagram of the novel joint is shown in Figure 16.

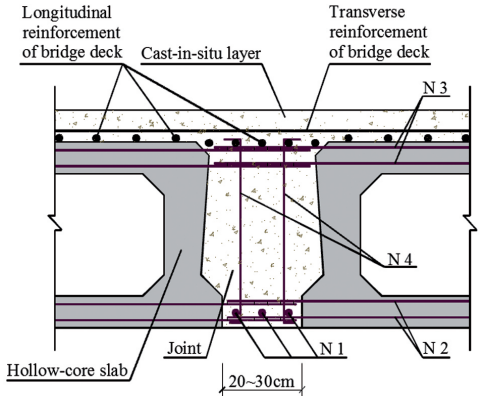

Fig. 16. Structure of novel joint

First, the bottom width of the novel joint was adjusted from the conventional 1-cm width to 20–30 cm.

Steel bars were then added to resist the load and strengthen the transverse connection of the structure in the joints: longitudinal reinforcement N1, bottom transverse reinforcement N2, top transverse reinforcement N3, and stirrup N4. Among them, N2 and N3 steel bars were correspondingly welded.

The advantages of the novel joint are as follows:

1. After increasing the bottom width of the novel joint, it becomes possible to vibrate the concrete of the joint; thus, the construction quality of the joint can be effectively guaranteed.
2. Because transverse reinforcement N1 and longitudinal reinforcement N2 are embedded at the bottom of the joint, joints have the ability to resist bending moments in the longitudinal and transverse directions.
3. Stirrups enhanced the shear resistance of the joint.
4. The corresponding welding of N2 and N3 steel bars strengthens the transverse connection between the hollow-core slabs.

4.2. Analysis of novel joints

The novel joint structure was used to optimise the pretensioned hollow-core slab model of the second and third parts of the simply supported assembly.

The bottom width of the joint between the hollow-core slabs was adjusted from 1 to 20 cm. The specific conditions for adding steel bars in the joints are N1, N2, N3, and N4 steel bars with diameters of 22, 16, 16, and 12 mm, respectively. The strength grade of all the steel bars was HRB400, and the yield strength was 400 MPa.

The loads and construction stages are the same as in the aforementioned model except that the equivalent cooling of CS is taken as 9.5°C after calculation.

In *stage iv*, cracks occurred in joints J1, J2, and J3. Among them, J1 had the largest number of cracks. The vertical cracks of J1 are mainly distributed in the range of 3/8–5/8 span (Figure 17a). The cracks only appeared on the bottom of the joints, and the middle and upper parts of the joints showed no crack formation (Figure 17b). Compared with Figure 15, the degree of crack development is greatly reduced, indicating that the reinforcement of the novel joint structure can better ensure the strength of the joint.

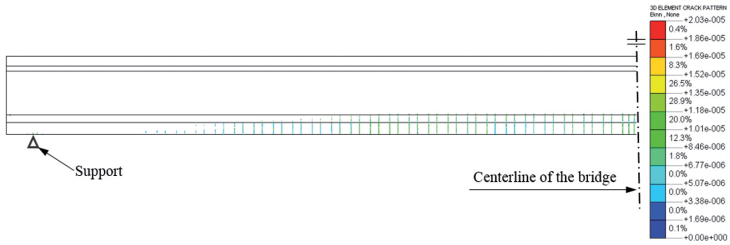

(a) Semi-elevation view of crack

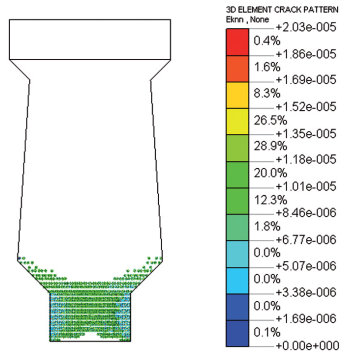

(b) Cracks at the mid-span cross section

Fig. 17. Cracks distribution of novel joint 1 in *stage iv*

The novel joint is designed according to reinforced concrete rather than a prestressed structure, and therefore will result in the formation of cracks. In *stage iv*, the maximum tensile stress of the longitudinal reinforcement and transverse reinforcement in the novel joint J1 is 8.99 MPa and 10.53 MPa respectively, and the maximum tensile stress of the novel joint J1 is 1.03 MPa. The tensile stress at the novel joint is mainly borne by the steel bar. The maximum tensile stress of the stirrups arranged in the novel joint J1 is 24.09 MPa. Since the joint is not only subjected to flexural stress but also to shear stress under the load, it is necessary to arrange stirrups to prevent shear failure to the novel joint. Because the steel bars of the novel joint configuration provide flexural and crack resistance, the crack

expansion of the joint is well controlled. Therefore, the novel joint can better ensure the rigidity and strength of the joint structure and can effectively ensure the transverse integrity of the fabricated hollow-core slab.

4.3. Design method of novel joints

Novel joints have flexural strength owing to the configuration of the steel bars. Therefore, the design method of longitudinal tensile reinforcement N1 should be clear.

Generally, the postprocessing function of three-dimensional finite element software only provides the results of stress and strain. The displacement, bending moment, axial force, and shear force of the structure cannot be obtained directly. However, the design of the joints requires the bending moment of each load.

Midas/FEA provides the sum of the local internal forces' function to extract the total internal force of the specified section of the solid element. By taking J1 as an example, the method of internal force extraction is explained as follows [41–43]:

First, only the elements of J1 are activated, and the target section is determined through three points.

Then the internal force is extracted by the *Sum of Local Internal Forces* function and F_x (axial force in X direction), F_y (shear force in Y direction), F_z (shear force in Z direction), M_x (bending moment around X axis), M_y (bending moment around Y axis) and M_z (bending moment around Z axis) of the section can be output, as shown in Figure 18.

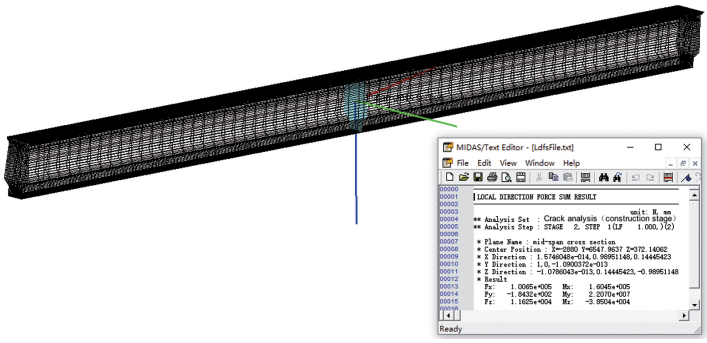

Fig. 18. Internal force integral of specified cross section

5. Conclusion

In this paper, a new type of joint was proposed based on the force mechanism of a conventional joint. The main conclusions are as follows:

1. In conventional joints, the CS development difference between the joints and prefabricated hollow-core slabs has an important influence on the stress of the joints. The greater the difference of the CS development age, the greater the is tensile stress in

the joints. For example, when the age difference is 2 years, the tensile force of the joint reaches 7.28 MPa.

2. Although VL and TG are secondary factors for the development of joint cracks, they are important for the determination of the upward development of cracks.
3. When bridge construction is completed, the conventional joints are in a very unfavourable stress state, the cracks in the middle and lower parts are penetrated, and local cracks appear in the middle and upper parts.
4. The new type of joint not only solves the problem of concrete vibration but also has good mechanical performance owing to the configuration of steel bars. The joint cracks were effectively controlled and only appear at the bottom of the novel joints. In addition, no cracks are formed in the middle and upper parts of the novel joints.

Acknowledgements

This study was funded by the Scientific Research Project of the Educational Department of Liaoning Province (LNZD 202005) and the Project of the MOE Key Lab of Disaster Forecast and Control in Engineering of Jinan University (20200904005). The authors would like to thank Editage (http://www.editage.cn) for English language editing.

References

[1] P. Kankeri, S.S. Prakash, "Efficient hybrid strengthening for precast hollow core slabs at low and high shear span to depth ratios", *Composite Structures*, 2017, vol. 170, pp. 202–214; DOI: 10.1016/j.compstruct.2017.03.034.

[2] P. Kankeri, S.S. Prakash, "Experimental evaluation of bonded overlay and NSM GFRP bar strengthening on flexural behavior of precast prestressed hollow core slabs", *Engineering Structures*, 2016, vol. 120, pp. 49–57; DOI: 10.1016/j.engstruct.2016.04.033.

[3] E. Cuenca, P. Serna, "Failure modes and shear design of prestressed hollow core slabs made of fiber-reinforced concrete", *Composites Part B: Engineering*, 2013, vol. 45, no. 1, pp. 952–964; DOI: 10.1016/j.compositesb.2012.06.005.

[4] H. Cho, M. Park, H. Ju, J. Oh, Y. Oh, K.S. Kim, "Shear Strength Reduction Factor of Prestressed Hollow-Core Slab Units Based on the Reliability Approach", *Advances in Materials Science and Engineering*, 2017, vol. 2017, pp. 1–11; DOI: 10.1155/2017/8280317.

[5] N. Staszak, T. Garbowski, B. Ksit, "Application of the Generalized Nonlinear Constitutive Law to Hollow-Core Slabs", *Archives of Civil Engineering*, 2022, vol. 68, no. 2, pp. 125–145; DOI: 10.24425/ace.2022.140633.

[6] M. Kalimur Rahman, I.A. Mahmoud, M.H. Baluch, "Finite Element Modeling of Prestressed Hollow Core Slab Strengthened with CFRP Sheets in Flexure and Shear", *Key Engineering Materials*, 2008, vol. 400-402, pp. 531–536; DOI: 10.4028/www.scientific.net/KEM.400-402.531.

[7] N.G. Wariyatno, Y. Haryanto, G.H. Sudibyo, "Flexural Behavior of Precast Hollow Core Slab Using PVC Pipe and Styrofoam with different Reinforcement", *Procedia Engineering*, 2017, vol. 171, pp. 909–916; DOI: 10.1016/j.proeng.2017.01.388.

[8] E. Brunesi, R. Nascimbene, "Numerical web-shear strength assessment of precast prestressed hollow core slab units", *Engineering Structures*, 2015, vol. 102, pp. 13–30; DOI: 10.1016/j.engstruct.2015.08.013.

[9] M. Gizejowski, W. Barcewicz, W. Salah, "Finite Element Modelling of the Behaviour of a Certain Class of Composite Steel-Concrete Beam-to-Column Joints", *Archives of Civil Engineering,* 2010, vol. 56, no. 1, pp. 19–56; DOI: 10.2478/v.10169-010-0002-0.

[10] G.H. Ahmed, O.Q. Aziz, "Shear strength of joints in precast posttensioned segmental bridges during 1959–2019, review and analysis", *Structures*, 2019, vol. 20, pp. 527–542; DOI: 10.1016/j.istruc.2019.06.007.

[11] S.Z. Park, K.J. Hong, S.W. Lee, "Behavior of an adhesive joint under weak-axis bending in a pultruded GFRP bridge deck", *Composites Part B*, 2014, vol. 63, pp. 123–140; DOI: 10.1016/j.compositesb.2014.04.002.

[12] B. Sun, R. Xiao, W. Ruan, P. Wang, "Corrosion-induced cracking fragility of RC bridge with improved concrete carbonation and steel reinforcement corrosion models", *Engineering Structures*, 2020, vol. 208, art. ID 110313; DOI: 10.1016/j.engstruct.2020.110313.

[13] M. Adel, P. Jiradilok, K. Matsumoto, K. Nagai, "Evaluation of crack-bridging strength degradation in SFRC structural beams under flexural fatigue", *Composite Structures*, 2020, vol. 244, art. ID 112267; DOI: 10.1016/j.compstruct.2020.112267.

[14] F. Liu, J. Zhou, "Experimental Research on Fatigue Damage of Reinforced Concrete Rectangular Beam", *KSCE Journal of Civil Engineering*, 2018, vol. 22, no. 9, pp. 3512–3523; DOI: 10.1007/s12205-018-1767-y.

[15] Y. Zhong, "Study on the Hinge Joint Model Experiment of Hollow Slab Beam Bridge", M.A. thesis, Chang'an University, China, 2008.

[16] P. Liu, "Study on Behaviors of Hinge Joints for Fabricated Reinforced Concrete Simply-supported Plate Girder Bridges", M.A. thesis, Tsinghua University, China, 2010.

[17] X. Zhang, "The precast hollow-cored slab bridge transverse joint design and improvement methods", M.A. thesis, Jilin University, China, 2017.

[18] M.A. Bajaber, I.Y. Hakeem, "UHPC evolution, development, and utilization in construction: a review", *Journal of Materials Research and Technology*, 2021, vol. 10, pp. 1058–1074; DOI: 10.1016/j.jmrt.2020.12.051.

[19] T. Zdeb, "Ultra-high performance concrete – properties and technology", *Bulletin of the Polish Academy of Sciences: Technical Sciences*, 2013, vol. 61, no. 1, pp. 183–193; DOI: 10.2478/bpasts-2013-0017.

[20] O. Gunes, S. Yesilmen, B. Gunes, F. Ulm, "Use of UHPC in Bridge Structures: Material Modeling and Design", *Advances in Materials Science and Engineering*, 2012, vol. 2012, pp. 1–12; DOI: 10.1155/2012/319285.

[21] H. Jiang, X. Dong, Z. Fang, J. Xiao, Y. Chen, "Experimental Study on Shear Behavior of a UHPC Connection Between Adjacent Precast Prestressed Concrete Voided Beams", *Journal of Bridge Engineering*, 2020, vol. 25, no. 12; DOI: 10.1061/(ASCE)BE.1943-5592.0001644.

[22] Y. Jiqiu, G. Benjamin, "Full-Scale Testing of Shear Key Details for Precast Concrete Box-Beam Bridges", *Journal of Bridge Engineering*, 2016, vol. 21, no. 9; DOI: 10.1061/(ASCE)BE.1943-5592.0000906.

[23] A.A. Semendary, K.K. Walsh, E.P. Steinberg, "Early-Age Behavior of an Adjacent Prestressed Concrete Box-Beam Bridge Containing UHPC Shear Keys with Transverse Dowels", *Journal of Bridge Engineering*, 2017, vol. 22, no. 5, art. ID 4017007; DOI: 10.1061/(ASCE)BE.1943-5592.0001034.

[24] H.H. Hussein, S.M. Sargand, F.T. Al Rikabi, E.P. Steinberg, "Laboratory Evaluation of Ultrahigh-Performance Concrete Shear Key for Prestressed Adjacent Precast Concrete Box Girder Bridges", *Journal of Bridge Engineering*, 2016, vol. 22, no. 2, art. ID 4016113; DOI: 10.1061/(ASCE)BE.1943-5592.0000987

[25] M.A. Issa, et al., "Performance of Transverse Joint Grout Materials in Full-Depth Precast Concrete Bridge Deck Systems", *PCI Journal*, 2003, vol. 48, no. 4, pp. 92–103; DOI: 10.15554/pcij.07012003.92.103.

[26] W. Shi, B. Shafei, Z. Liu, B.M. Phares, "Early-age performance of longitudinal bridge joints made with shrinkage-compensating cement concrete", *Engineering Structures*, 2019, vol. 197, art. ID 109391; DOI: 10.1016/j.engstruct.2019.109391.

[27] N. Liu, Y. Yang, "Analysis and Optimization Design Method of Diseases of Hinged Plate Bridge", *Journal of Highway and TransportationResearch and Development*, 2016, vol. 33, no. 02, pp. 73–81.

[28] Y. Wang, "Research on design method of transverse joint for precast hollow concrete slab bridge", M.A. thesis, Harbin Institute of Technology, China, 2015.

[29] G. Annamalai, "Shear Strength of Post-Tensioned Grouted Keyed Connections", *PCI Journal*, 1990, vol. 35, no. 3, pp. 64–73; DOI: 10.15554/pcij.05011990.64.73.

[30] T. Yamane, M.K. Tadros, P. Arumugasaamy, "Short to medium span precast prestressed concrete bridges in Japan", *PCI Journal*, 1994, vol. 39, no. 2, pp. 74–100; DOI: 10.15554/pcij.03011994.74.100.

[31] I. Khan, A. Castel, R.I. Gilbert, "Tensile creep and early-age concrete cracking due to restrained shrinkage", *Construction and Building Materials*, 2017, vol. 149, pp. 705–715; DOI: 10.1016/j.conbuildmat.2017.05.081.

[32] S. Asamoto, A. Ohtsuka, Y. Kuwahara, C. Miura, "Study on effects of solar radiation and rain on shrinkage, shrinkage cracking and creep of concrete", *Cement and Concrete Research*, 2011, vol. 41, no. 6, pp. 590–601; DOI: 10.1016/j.cemconres.2011.03.003.

[33] S. Zhang, E. Hamed, "Application of various creep analysis methods for estimating the time-dependent behavior of cracked concrete beams", *Structures*, 2020, vol. 25, pp. 127–137; DOI: 10.1016/j.istruc.2020.02.029.

[34] K. Flaga, "The influence of concrete shrinkage on durability of reinforced structural members", *Bulletin of the Polish Academy of Sciences Technical Sciences,* 2015, vol. 63, no. 1, pp. 15–32; DOI: 10.1515/bpasts-2015-0002.

[35] M. Gołdyn, "Shear capacity of the interface between concretes cast at different time in the light of experimental investigations and codes of practice", *Archives of Civil Engineering*, 2022, vol. 68, no. 1, pp. 275–298; DOI: 10.24425/ace.2022.140168.

[36] Ministry of Transport of the People's Republic of China, "JTG D60-2015 General Code for Design of Highway Bridges and Culverts", China, 2015.

[37] F. PH, "Computational aspects of biaxial stress in plain and reinforced concrete", Ph.D. thesis, TU Delft: Department of Civil Engineering, Netherlands, 1993.

[38] D.A. Hordijk, "Local approach to fatigue of concrete", PhD. thesis. TU Delft: Department of Civil Engineering, Netherlands, 1991.

[39] Midas IT(Beijing) Co.,Ltd., "MidasFEA Analysis and Algorithm Manual". [Online]. Available: http://www.MIDASUser.com. [Accessed: 6. Feb. 2022].

[40] Ministry of Housing and Urban-Rural Development of the People's Republic of China, "GB50010-2010 Code for design of concrete structures", China, 2010.

[41] X. Xue, C. Zang, J. Zhou, H. Zhang, "Numerical Investigation of Distribution Laws of Shear Force in Box Girder Webs", *Advances in Materials Science and Engineering*, 2019, vol. 2019, pp. 1–14; DOI: 10.1155/2019/9865989.

[42] X. Xue, J. Zhou, X. Hua, H. Li, "Analysis of the Generating and Influencing Factors of Vertical Cracking in Abutments during Construction", *Advances in Materials Science and Engineering*, 2018, vol. 2018, pp. 1–13; DOI: 10.1155/2018/1907360.

[43] X. Xue, M. Wu, Z. Li, P. Zhou, "Numerical Analysis of Dead Load Shear Force Distribution in Webs of Multicell Inclined Web Box-Girder Bridge", *Advances in Civil Engineering*, 2020, vol. 2020, pp. 1–10; DOI: 10.1155/2020/9670704

Received: 2022-06-18, Revised: 2022-08-23